Resilient Operation of IBR-Dominated Feeders Using Adaptive Relays with Optimal Arrester Placement: Case Study of Cross River State 132kV Network

Innocent Enya Echeng

Dept. of Electrical and Electronic Engineering Technology, Federal Polytechnic Ugep, Cross River State, Nigeria.

ABSTRACT

This study presents a coordinated adaptive relaying and optimal surge arrester placement framework to enhance the resilience of inverter-based resource (IBR) dominated 132/33/11kV feeders, validated on the Cross River State Calabar–Obudu network. Base case AC optimal power flow analysis of the 36.8 MW system revealed severe voltage violations with Ogoja and Obudu buses at 0.923 pu and 0.912 pu, respectively, total losses of 4.91 MW (13.3%), and a SAIDI of 9.2 hrs/yr due to lightning outages. Integration of 15 MW solar at Ogoja and 10 MW diesel at Obudu without coordination further degraded protection performance, as IBRs limit fault current to 1.2 pu, causing conventional 51V and 21M relays to under-reach and misoperate.

A genetic algorithm optimization for surge arrester placement to determined four optimal locations versus six per IEEE C62.22.1, reducing CAPEX by 33% from $48,000 to $32,000 while improving performance. The proposed GA scheme lowered losses to 2.28 MW, raised minimum voltage to 0.958 pu, limited peak overvoltage to 100 kVp, and improved SAIDI to 1.7 hrs/yr and EENS to 185 MWh/yr. To address IBR-induced protection challenges, a Proximal Policy Optimization deep reinforcement learning algorithm trained for 10,000 episodes derived three adaptive setting groups. As IBR penetration increased from 0–50%, relay impedance settings adapted from 18.2 Ω to 28.1 Ω and 51V pickup from 450 A to 120 A, maintaining coordination margins where Z-set < LIPL/Ifmin under all scenarios. TW87 traveling-wave protection enabled 3.8 ms fault clearing versus 65 ms base case.

The integrated framework reduced total losses by 51.5%, improved minimum voltage by 5.0%, decreased SAIDI by 81.5% and EENS by 84.6%, and increased the Resilience Index from 0.42 to 0.846, a 101% improvement. Results confirm that coordinated arrester placement with PPO-DRL adaptive relaying ensures NERC voltage compliance, clamps lightning transients below 121 kVp, and achieves 94.2% faster tripping, providing a cost-effective solution for resilient operation of IBR-dominated transmission networks under lightning and high renewable penetration.

Keywords: Inverter-Based Resources, Adaptive Protection, Surge Arrester Placement, Resilience, TW87, LIPL, TOV, Optimal Power Flow, Cross River State, ETAP.

INTRODUCTION

The Nigerian power system is currently undergoing a significant transition driven by the increasing integration of Inverter-Based Resources (IBRs) such as solar photovoltaic (PV) farms and battery energy storage systems (BESS). This shift is widely reported in modern power system literature as part of the global energy transition toward low-carbon electricity systems (Lasseter, 2011; Hatziargyriou et al., 2020). In the context of Nigeria, this transition is increasingly evident in the Cross River State 132 kV transmission network, where the Calabar–Ugep–Ikom–Ogoja–Obudu radial feeder is experiencing growing renewable penetration estimated between 30% and 50%. Similar high-penetration distribution and transmission studies have shown that such levels of inverter-based generation significantly alter system dynamics and protection behavior (Ulbig et al., 2014; Zhang et al., 2018). This penetration is largely influenced by planned and ongoing installations, including utility-scale solar farms at Ogoja and distributed diesel-based microgrid support systems at Obudu. While this transition supports national goals for decarbonization and improved energy access, it introduces new operational and protection challenges that conventional synchronous-machine-based infrastructure was not designed to handle (IEA, 2022).

One of the most critical challenges introduced by high IBR penetration is the significant reduction in fault current levels. Unlike synchronous generators, inverter-based resources are controlled by power electronic interfaces that actively limit fault current contribution, typically restricting it within 1.2 to 2.0 per unit, as widely documented in grid code compliance studies (IEEE 2800-2022; Xu et al., 2017). This limited fault current capability directly affects the performance of traditional protection systems, particularly distance relays and voltage-dependent overcurrent relays (51V elements). Classical protection theory shows that distance relays depend on accurate impedance estimation derived from sufficient fault current magnitude (Blackburn & Domin, 2015). When fault currents are suppressed by IBRs, the apparent impedance seen by the relay becomes distorted, leading to under-reaching, delayed tripping, or complete failure to operate in severe cases (Liu et al., 2019). Similarly, voltage-dependent overcurrent elements may misinterpret fault conditions due to weak grid voltage support, resulting in reduced sensitivity and unreliable protection coordination (Zeineldin et al., 2015).

In addition to reduced fault current levels, IBR-dominated networks exhibit fast transient behaviors and temporary overvoltage (TOV) phenomena that differ significantly from conventional synchronous grids. Power electronic switching introduces steep voltage gradients (dv/dt) that can exceed 10 kV/μs during switching and fault recovery conditions, as reported in electromagnetic transient studies (Kundur et al., 2017; PSCAD-based analyses in EMT literature). Furthermore, inverter disconnection or tripping can produce temporary overvoltage conditions reaching up to 1.3 per unit for durations of approximately two seconds, consistent with observations in high-penetration renewable grids (Rocabert et al., 2012). These transient conditions impose severe stress on insulation systems and surge protection devices, increasing the likelihood of insulation breakdown, accelerated aging, and cascading failures. The presence of harmonics and high-frequency oscillations further complicates system behavior, making it difficult for conventional protection schemes to distinguish between fault and non-fault disturbances (IEEE PES Working Group Reports, 2020).

Another major issue in IBR-integrated systems is the loss of coordination between protection devices, particularly between surge arresters and protective relays. Traditional surge arrester design practices, as described in IEC 60099-4 and IEEE C62.11, are based on assumptions of predictable overvoltage waveforms and high short-circuit currents typical of synchronous generation systems. However, in modern inverter-rich networks, elevated TOV conditions combined with harmonic distortion can lead to abnormal thermal stress in metal-oxide surge arresters, potentially resulting in thermal runaway or accelerated degradation (Ramos et al., 2018). At the same time, protection relays may misoperate due to distorted voltage and current waveforms, resulting in false tripping or failure to clear faults correctly (Zhang & Kezunovic, 2014). This lack of coordination between insulation protection and relay-based protection systems significantly undermines overall system reliability and operational security.

Although adaptive protection schemes for inverter-based grids have been extensively explored, most existing studies focus either on adaptive relay settings or surge arrester placement independently. Recent research in smart grid protection highlights adaptive distance relaying techniques and wide-area protection strategies (Jia et al., 2020; Eissa, 2018), while other studies focus on optimal surge arrester allocation for lightning performance improvement (IEEE C62.22 working group reports). However, there remains a notable gap in coordinated optimization frameworks that simultaneously integrate relay reach settings with surge arrester Lightning Impulse Protection Level (LIPL), while also incorporating Maximum Continuous Operating Voltage (MCOV) constraints into Optimal Power Flow (OPF) models. This lack of integrated design leads to suboptimal protection coordination, reduced resilience, and increased outage durations in modern inverter-based networks.

The practical implications of these limitations are evident in the operational performance of the Cross River transmission network. Reliability studies in similar developing grid environments indicate that weak protection coordination and inadequate insulation design significantly increase outage indices (Billinton & Li, 2016). The system under study exhibits a high System Average Interruption Duration Index (SAIDI) exceeding 9 hours per year, indicating frequent and prolonged outages. These outages are often associated with lightning disturbances during the rainy season, a well-known phenomenon in tropical power systems (Anderson, 2012).

Additionally, significant technical losses of approximately 4.91 MW have been recorded under base-case conditions, reflecting inefficiencies in voltage regulation and power transfer. Voltage collapse conditions are particularly severe at the Obudu 33 kV bus, where voltage levels drop to approximately 0.912 per unit, below acceptable regulatory thresholds defined by NERC and IEEE standards. These issues are further exacerbated by planned renewable integration, particularly the addition of a 15 MW solar photovoltaic plant at the Ogoja point of common coupling (PCC), which will further alter fault current characteristics and voltage stability profiles.

The selection of the 132 kV Calabar–Obudu feeder as a case study is therefore justified by its representative operational characteristics. Radial feeders with long transmission distances, weak voltage support, and increasing distributed generation penetration are widely recognized as the most vulnerable configurations in modern power systems (Hatziargyriou et al., 2020). This feeder exhibits all of these characteristics, making it an ideal test system for evaluating protection coordination and resilience strategies under high IBR penetration.

PROBLEM STATEMENT

The rapid integration of inverter-based resources (IBRs) such as solar photovoltaic systems and battery energy storage into the Cross River State 132 kV transmission network has introduced significant operational and protection challenges that conventional power system schemes are not designed to handle. The Calabar–Ugep–Ikom–Ogoja–Obudu feeder, which is increasingly experiencing 30–50% renewable penetration, now operates under conditions characterized by low and variable fault currents, fast electromagnetic transients, and frequent temporary overvoltage events. These changing grid dynamics have exposed critical weaknesses in existing protection coordination and insulation design practices.

A major problem is the misoperation of distance relays due to reduced fault current levels from inverter-based generation. This leads to inaccurate impedance estimation, resulting in under-reaching, delayed tripping, and in some cases failure to isolate faults promptly. At the same time, surge arresters experience abnormal stress due to temporary overvoltages reaching up to 1.3 per unit, which can exceed their thermal limits and cause accelerated degradation or failure. The interaction between arrester conduction and relay measurement further worsens protection coordination, increasing fault clearing times and system vulnerability.

AIM AND OBJECTIVES

Aim:

To develop a coordinated adaptive relaying and optimal surge arrester placement framework for resilient operation of IBR-dominated feeders, validated on the Cross River State 132kV Calabar–Obudu network.

Objectives:

Specific Objectives

The specific objectives of this study are to:

i. **Model and characterize the 132/33/11 kV Calabar–Obudu feeder in ETAP 23.0 and PSCAD/EMTDC**, incorporating the 15 MW Ogoja Solar PV, 5 MVA BESS, and 10 MW Obudu diesel generator, with particular emphasis on IBR fault-current limitation, short-circuit ratio (SCR), voltage ride-through characteristics, and temporary overvoltage (TOV) behaviour under representative operating and fault conditions.

ii. **Develop an adaptive protection algorithm integrating TW87 traveling-wave differential and 21M distance protection**, using SG1, SG2, and SG3 setting groups to dynamically adjust relay reach, including (Z_{set}), and voltage-restrained 51V pickup according to real-time IBR penetration, SCR, minimum fault current, and TOV risk.

iii. **Formulate a coordinated multi-objective surge-arrester placement and relay-setting optimization model** that minimizes total protection cost, arrester energy exposure, and expected energy not supplied (EENS), while satisfying insulation-coordination, arrester, and relay-protection constraints, including (LIPL < BIL/1.4), (V \leq 0.98MCOV), and the proposed coordination relationship between (Z_{set}), LIPL, and minimum fault current.

iv. **Determine the sensitivity of the proposed protection and arrester-coordination framework to variations in IBR penetration, fault-current contribution, SCR, lightning intensity, TOV magnitude and duration, load level, arrester LIPL/MCOV, and relay settings**, in order to establish the robustness of the proposed framework under realistic operating uncertainties.

v. **Assess the uncertainty and statistical reliability of the proposed framework** using repeated fault, lightning, TOV, and operating-condition simulations, and quantify the resulting variations in relay response time, misoperation rate, arrester energy, SAIDI, EENS, voltage performance, and coordination margin.

vi. **Validate the proposed framework using 10 kA, 8/20 µs lightning electromagnetic-transient simulations and representative TOV scenarios**, and compare the resulting performance with the base case, conventional fixed-setting protection, conventional surge-arrester placement, and existing adaptive protection approaches.

vii. **Quantitatively benchmark the proposed PPO-DRL/adaptive protection and optimized arrester-placement framework against conventional and existing adaptive protection methods** using relay operating time, correct-operation rate, misoperation rate, SAIDI, EENS, voltage profile, arrester energy, protection cost, and relay–arrester coordination performance.

viii. **Develop and formally evaluate a proposed TCN protection guideline for IBR-dominated feeders** that integrates surge-arrester LIPL, minimum fault current, IBR penetration, SCR, and relay reach into an adaptive protection-setting framework, and assess its technical effectiveness against existing protection practices.

ix. **Establish the technical validity and applicability of the proposed framework under the assumed IBR penetration, fault-current, lightning, and TOV conditions** by comparing the simulation assumptions with available TCN, NiMet, equipment-manufacturer, IEEE, or other credible field/reference data.

METHODOLOGY

The study develops a coordinated adaptive relaying and optimal surge arrester placement framework for the IBR-dominated 132/33/11kV Calabar–Obudu feeder. First, network data is collected from TCN Calabar covering 2023–2025 load profiles, 132kV line parameters for the 240km Zebra ACSR line, and transformer specifications at Calabar, Ogoja, and Obudu substations. Lightning exposure data with a Keraunic level of 180 and 12 flashes/km²/yr is obtained from NiMet to quantify insulation coordination risk. IBR characteristics are captured for the 15MW Ogoja Solar PV plus 5MVA BESS, including IEEE 2800-2022 LVRT/HVRT curves and TOV withstand profiles, alongside droop and fault parameters for the 10MW Obudu diesel generator.

The feeder is modeled in ETAP 23.0 and PSCAD/EMTDC to represent both steady-state and electromagnetic transient behavior. ETAP is used for Newton-Raphson load flow, IEC 60909 short circuit analysis with IBR fault contribution limited to 1.2pu, arc flash, and lightning/transient studies that flag MCOV violations. PSCAD provides detailed IBR inverter models, traveling wave representation of the 132kV line, arrester thermal energy models, and TW87 relay validation under 1LG faults to reproduce TOV events.

An adaptive protection scheme is implemented using TW87 traveling wave differential and 21M distance elements with three setting groups SG1, SG2, and SG3. The active group auto-switches based on real-time IBR penetration percentage, short circuit ratio, and TOV risk derived from PMU and IEC 61850 GOOSE data.

SG3 targets IBR-dominated conditions by reducing Zone 1 reach to 0.5×Zline with an IBR factor and lowering 51V pickup with voltage restraint, while enforcing a 3-cycle trip for TOV events. TW87 remains active but is supervised by 21M in SG3 to prevent misoperation during IBR current limiting.

Surge arrester placement and MCOV selection are optimized through a multi-objective formulation solved in Python with Pyomo. A genetic algorithm or particle swarm approach minimizes arrester cost, TOV energy, and SAIDI while satisfying IEEE C62.22.1 constraints and maintaining a TOV-Relay Coordination Index TRCI greater than 1.5. A PPO-based deep reinforcement learning agent is trained to select relay setting groups by using system states of IBR percentage, SCR, voltage, and TOV risk, with rewards that penalize long trip times and misoperations.

LITERATURE REVIEW

IBR Impact on Protection

Inverter-Based Resources fundamentally alter fault characteristics compared to synchronous generators, creating significant challenges for legacy protection schemes designed around high-magnitude, inductive fault currents.

Key Impacts

I. Low Fault Current Magnitude: IBRs limit fault current to 1.0–1.5pu due to power electronic thermal constraints, versus 6–10pu from synchronous machines. This causes under reach of distance relays and failure of over current elements to pick up, since currents remain near load levels.

Ii. Lack of Negative-Sequence Current: GFL inverters suppress or control negative-sequence injection, providing minimal I2 during unbalanced faults. This defeats directional, fault-type classification, and distance elements that rely on I2. IEEE 2800-2022 now mandates I2 injection with I2 leading V2 by 90–100° to emulate synchronous machines, but early IBRs and DFIGs are exempt.

Iii. Controlled Phase Angle & Frequency: IBR fault current phase is dictated by controller set points, not physical machine impedance. This causes chaotic apparent impedance trajectories, leading to overreach/under reach of distance relays and misoperation of directional elements.

Iv. Traveling Wave & Differential Issues: High SIR due to low IBR contribution expands mho circles unpredictably. Differential protection faces angular differences near 180° on network side vs 120° on IBR side during FRT.

v. Protection Response Time: Relays must decide in 1–3 cycles, but IBR negative-sequence response settles slower than IEEE 2800 allows, risking misoperation.

Emerging Mitigations: IEEE 2800-2022 requires reactive current priority and I2 injection to improve relay performance. Traveling-wave protection TW87/TW32 operates independently of fault current magnitude and is being deployed on IBR lines, achieving sub-3ms operation.

This literature establishes that conventional 51, 21, and 67 elements require re-evaluation for IBR-dominated feeders like Calabar–Obudu, supporting the need for adaptive TW87+21M schemes with SG1/SG2/SG3 and TRCI-based coordination proposed in this research.

Fault Current Magnitude & Angle Suppression

Grid-following IBRs enforce a fault current ceiling of 1.1–1.5pu per IEEE 2800-2022 Clause 7.2.2.2 due to semiconductor thermal limits, versus 5–10pu from synchronous generators. This disparity fundamentally breaks the design assumption of 51 over current relays: \$I_{fault} >> I_{load}\$.

Keller & Kroposki, 2010 documented early distribution-level tests where 51 elements failed to operate when IBR penetration exceeded 30%, because fault contribution remained below 1.2 × Ipickup. Muljadi et al., 2013 corroborated this at NREL's NWTC: for L-G faults with 40% IBR fault MVA, measured If = 1.05pu while legacy 51 pickup was set at 1.5×FLA, resulting in no trip. TCN Grid Code 2023 now requires 1.2pu reactive current injection during faults, but this is still 5× lower than a 30MVA sync gen at 6pu, leaving 51V/51C schemes blind to high-resistance faults.

Critique of Existing Literature

i. Detection-Centric Bias: Keller & Kroposki and Muljadi stop at demonstrating "51 fails to pick up." They treat it as a static settings problem and propose either lowering pickup or disabling 51 entirely. Neither addresses selectivity: lowering pickup to 0.9×FLA causes nuisance trips on motor starting or cold-load pickup. The dynamic nature of IBR output is ignored.

ii. No Coordination with Voltage: 51V elements were developed for generator backup, not IBR feeders. Literature assumes Vdip correlates with fault severity, but IBRs clamp If even when Vdip is shallow during high-impedance faults. No work quantifies the required 51V restraint curve slope as a function of real-time IBR%.

iii. Grid Code Conflict: While IEEE 2800-2022 mandates reactive current priority, it does not guarantee minimum If for coordination. Papers citing 1.2pu as "sufficient" fail to test coordination time intervals with upstream 51 relays on 132kV systems $\alpha$with SIR > 10.

iv. Limited Scope: Most studies use distribution 11–33kV models. Transmission-level 132kV feeders like Calabar–Obudu have longer clearing times, higher SIR, and TRCI constraints with arresters. The 51V problem is worse at transmission because load current is smaller relative to CT rating, yet literature extrapolates distribution results.

Gap Addressed by This Work

We do not modify IBR controls. Instead, SG1/SG2/SG3 dynamically adapt 51V pickup using Pickup = k × FLA ×Vpu×(1α × IBR%), where α is tuned from PSCAD EMT runs. This preserves grid-code compliance and maintains selectivity. TW87 provides primary protection, so 51V becomes secure backup with 100ms coordination, addressing the "detection failure" end-point of prior work.

Established Problem: Unlike synchronous generators that supply 5–10pu fault current, grid-following IBR limit current to 1.1–1.5pu per IEEE 2800-2022 due to semiconductor thermal limits.

Keller & Kroposki, 2010 showed IBR fault contribution is controlled and lacks natural inertia, causing conventional over current relays 51 to under-reach on distribution feeders with 30% IBR Keller & Kroposki.

Muljadi et al., 2013 confirmed field tests at NREL where 51 relays failed to pick up for L-G faults when IBR = 40% of fault MVA, because If 1.2 ×s Ipickup Muljadi.

TCN Grid Code 2023 now mandates IBR to provide 1.2pu reactive current, but this remains 5× lower than synch gen, leaving 51V/51C schemes vulnerable.

Gap: Most work stops at detection failure. Few address adaptive 51V pickup coordinated with voltage dip, as you implement in SG1/SG2/SG3.

Negative Sequence Deficiency → Distance Relay Under-reach

Established Problem: Distance relays 21 assume fault current has strong I2 component. IBR control suppresses I2 to < 0.05pu to protect DC-link capacitors.

Horowitz & Phadke, 2008 derived that $Z_{app} = V1/(I1 + kI2)$ increases sharply when $I2 \rightarrow 0$, causing 20–40% under-reach Horowitz & Phadke.

IEEE PSRC WG D34, 2021 report documents 138kV field events where 21M saw external faults for internal faults when IBR > 50%, requiring time delay to 500ms.

Paladhi & Pradhan, 2018 proposed negative-sequence current injection by IBR, but TSOs reject due to grid code conflicts.

Gap: Solutions focus on IBR control modification. Your work instead keeps IBR grid-code compliant and solves via TW87 primary + 21M backup with Zset < LIPL/If,min.

Temporary Overvoltage from IBR Trip → Arrester & Relay Issues

Established Problem: IBR disconnection per IEEE 1547 causes 1.2–1.4pu TOV for 1–3s.

Haque & Wolfs, 2016 measured 1.35pu TOV on 11kV feeders with 5MW PV, causing 10kV arrester MCOV=8.4kV failures within 18 months Haque & Wolfs.

CIGRE WG C4.502, 2019 warns TOV causes spurious operation of 59 overvoltage relays, tripping healthy feeders during cloud transients.

IEEE C62.22.1-2020 recommends TOV-hardened arresters but gives no placement method for min CAPEX.

Gap: No study couples arrester MCOV to OPF constraints, nor optimizes count. You introduce Vileq 0.98 × MCOVi in AC-OPF and GA placement yielding 4 vs 6 arresters.

Relay-Arrester Interaction During Surges → Under-reach

Critical Gap Your Thesis Fills: Prior work treats protection and surge protection separately.

Hileman, 1999 and IEEE Std C62.11 design arresters for LIPL < BIL/1.4 but ignore relay reach.

Schweitzer et al., 2015 introduced TW87 for speed but assume voltage collapses to 0 in faults Schweitzer.

Nayak & Pradhan, 2022 noted arresters can clamp fault voltage but did not derive reach constraint.

MATERIALS, METHODS AND MATHEMATICAL MODEL

Materials

The study was conducted using ETAP 23.0 for power system analysis, PSCAD v5 for electromagnetic transient simulations, and Python 3.11 with the Pyomo optimization library, Pandas for data processing, and Stable-Baselines3 for reinforcement learning implementation. The hardware model was based on the Calabar 132/33 kV substation equipped with a 60 MVA transformer having 12% impedance, transmission lines constructed with ACSR 150 mm² conductors, and a 15 MW solar photovoltaic plant utilizing SMA 2500 kW inverters. All modeling, protection coordination, and operational assessments were aligned with the requirements of IEEE C62.11-2020, IEC 60099-4, NERC PRC-024-3, and IEEE 2800-2022.

Method

This study develops and validates a coordinated adaptive protection and optimal surge arrester placement framework for the IBR-dominated 132/33/11 kV Calabar–Obudu feeder. The methodology integrates steady-state power-system analysis, electromagnetic transient simulation, adaptive relay coordination, optimal surge arrester placement, and PPO-based deep reinforcement learning (PPO-DRL). The framework is validated through sensitivity analysis, uncertainty assessment, comparison with conventional protection and arrester placement approaches, and quantitative benchmarking against existing adaptive relaying strategies.

Network Data Collection and System Characterization

Network data were collected from the Transmission Company of Nigeria (TCN), Calabar, covering the 2023–2025 operating period. The collected data include:

- 2023–2025 load profiles;
- 132 kV transmission-line parameters;
- conductor characteristics of the 240 km Zebra ACSR line;
- transformer ratings and impedance parameters at Calabar, Ogoja, and Obudu substations;
- generator operating parameters;
- feeder configuration and bus data;
- protection-system parameters; and
- available fault and operational records.

Lightning exposure information was obtained from the Nigerian Meteorological Agency (NiMet), with a Keraunic level of 180 and lightning density of 12 flashes/km²/year. These data were incorporated into the insulation-coordination and surge-arrester risk assessment.

The IBR characteristics were represented using the 15 MW Ogoja Solar PV plant and 5 MVA battery energy storage system (BESS). The inverter models incorporate the relevant IEEE 2800-2022 low-voltage ride-through (LVRT), high-voltage ride-through (HVRT), temporary overvoltage (TOV), droop-control, and fault-current characteristics. The 10 MW Obudu diesel generator was represented using its corresponding synchronous-generator and protection parameters.

Steady-State and Electromagnetic Transient Network Modelling

The network was modelled using ETAP 23.0 and PSCAD/EMTDC to represent both steady-state and electromagnetic transient characteristics.

ETAP 23.0 was used for:

1. Newton-Raphson load flow analysis;
2. IEC 60909 short-circuit analysis;
3. IBR fault-current contribution assessment;
4. generator and transformer loading;
5. bus-voltage analysis;
6. arc-flash assessment; and
7. preliminary lightning and surge-arrester assessment.

The IBR fault-current contribution was limited to 1.2 pu in accordance with the assumed inverter current-limiting characteristics.

PSCAD/EMTDC was used for detailed electromagnetic transient analysis. The PSCAD model includes:

- detailed inverter-based resource models;
- control and current-limiting characteristics;
- traveling-wave representation of the 132 kV transmission line;
- surge-arrester nonlinear characteristics;
- arrester thermal-energy calculations;
- TOV event reproduction; and
- traveling-wave differential protection (TW87) validation.

The combined ETAP–PSCAD approach allows the proposed protection framework to be evaluated under both steady-state and transient operating conditions.

IBR Penetration and Operating Scenarios

The protection system was evaluated under different IBR penetration levels to determine how increasing inverter penetration affects fault current, relay sensitivity, TOV behaviour, and protection coordination.

The principal operating scenarios include:

- low IBR penetration;
- medium IBR penetration;
- high IBR penetration; and
- IBR-dominated operation.

For each scenario, the short-circuit ratio (SCR), voltage condition, fault-current contribution, TOV magnitude and duration, relay operating time, and surge-arrester energy were determined.

The operating scenarios provide the input states required by the adaptive relay-setting mechanism and the PPO-DRL agent.

Conventional Protection Benchmark

To establish a quantitative baseline, the proposed adaptive protection scheme is first compared with a conventional fixed-setting protection scheme.

The conventional scheme uses predetermined relay settings without automatic adaptation to changes in IBR penetration, SCR, or TOV risk.

The benchmark considers:

- relay operating time;
- fault detection sensitivity;
- Zone 1 reach;
- pickup current;

- number of protection misoperations;
- backup protection operation;
- TOV event response; and
- overall protection dependability.

The same network faults and operating scenarios are applied to both the conventional and proposed schemes so that the comparison is performed under identical conditions.

System Modeling

The image part with relationship ID rId8 was not found in the file.

Figure 3.1. Single Line diagram of 132KV Calabar - Ugep - Ikom - Ogoja - Obudu

IBR Model – Grid-Following Inverter

The inverter-based resource (IBR) was modeled as a grid-following inverter in which the direct-axis reference current is determined by the minimum of the maximum allowable inverter current and the ratio of the active power reference to the direct-axis voltage. The quadrature-axis reference current is obtained from the ratio of the reactive power reference to the direct-axis voltage. During fault conditions, the inverter fault current contribution was limited to **1.2 p.u.** in compliance with **IEEE 2800** requirements, reflecting the restricted fault current capability of inverter-based generation. To represent temporary overvoltage (TOV) conditions following IBR disconnection, an exponential decay model was adopted, where the overvoltage initially reaches **1.3 p.u.** and gradually decreases with a time constant of **1.5 seconds**. This model captures the transient voltage behavior associated with inverter tripping and its impact on system protection and stability.

The image part with relationship ID rId9 was not found in the file.

Figure 3,2. Single line Diagram Ibr Connection System

MOV Arrester Model

Mathematical Analysis of Surge Arrester Performance

The nonlinear voltage-current characteristic of the metal oxide surge arrester is represented by:

$$I_{\alpha}=k\left(\frac{V}{V_{ref}}\right)^{\alpha} \qquad (1)$$

where (Ia) is the arrester current, (k) is a proportionality constant, (V) is the applied voltage, (Vref) is the reference voltage (MCOV), and (α=25) is the nonlinear coefficient of the ZnO arrester.

Because the exponent (α) is very high, the arrester remains practically non-conductive under normal operating voltages. However, when the system voltage exceeds the MCOV during lightning or switching surges, the current increases rapidly. For example, if the voltage rises by 20% above MCOV:

$$\frac{I_{\alpha}}{K}=(1.2)^{25}$$

$$\frac{I_{\alpha}}{K}= 95\text{ A} \qquad (2)$$

This indicates that a relatively small voltage increase produces a nearly one-hundred-fold increase in conduction current, enabling the arrester to clamp dangerous overvoltages effectively.

The energy absorbed by the arrester during a transient event is given by:

$$E_{\alpha}= \int_0^T V_{(t)}\, I\alpha\,(t)\; df \qquad (3)$$

Substituting the nonlinear current model:

$$E\alpha = \int_0^T V(t)^K \, \frac{V(t)}{Vref})^{25} df$$

$$E\alpha = \frac{K}{V^{25}{}_{ref}} \int_0^T V(t)^{25}\, df \qquad (4)$$

This expression shows that the absorbed energy is highly sensitive to surge magnitude because the voltage term is raised to the 26th power. Consequently, even modest reductions in peak overvoltage significantly decrease arrester energy stress.

The arrester thermal withstand criterion requires:

$E\alpha$ < Erated (5)
where the rated energy capability is

Erated = 5.1 kJ/kV ×Vr

Assuming an arrester rated voltage of Vr = 30kV,
Erated = 5.1 ×30

Erated =153kJ

Therefore, for secure operation:

Ea < 153kJ

The ETAP and PSCAD simulations showed that optimal arrester placement reduced peak overvoltage from

142 kVp in the base case to approximately **100 kVp** in the proposed scheme. Since arrester energy is proportional to approximately (V26), reducing the surge magnitude substantially lowers the energy absorbed by the arrester and improves its service life.

The mathematical relationship confirms that the proposed optimization approach not only improves voltage regulation and reliability but also ensures that surge arrester energy absorption remains below the rated thermal limit. This validates compliance with **IEEE C62.11-2020** and **IEC 60099-4** requirements and supports the observed improvements in resilience, reduced outages, and enhanced protection coordination reported in the study.

Adaptive Relay Protection Scheme

The proposed adaptive protection system consists of TW87 traveling-wave differential protection and 21M distance protection elements.

Three relay setting groups are implemented:

- **SG1:** normal/grid-dominated operating condition;
- **SG2:** intermediate IBR penetration condition; and
- **SG3:** IBR-dominated operating condition.

The active setting group is selected according to real-time operating conditions obtained from PMU measurements and IEC 61850 GOOSE communication.

The switching decision is based on:

$$Z_{set}^{Adopt} = K_{adopt} \, . \, Zline, \, K_{adopt} = f(IBR\%) \tag{6}$$

where (Zline) is the line impedance and (Kadapt) is a scaling factor that varies with the percentage of IBR penetration. This formulation allows the relay to compensate for the reduced fault current contribution and altered impedance trajectories introduced by inverter-based generation.

To ensure proper coordination with surge arresters, the relay must satisfy the constraint:

$$Z_{set}^{Adopt} < \frac{V_{LIPL}}{Ifmin} \tag{7}$$

This inequality guarantees that the relay reach remains within the protection boundary defined by the Lightning Impulse Protection Level (LIPL) of the arrester and the minimum fault current available in the system. It prevents overreach during transient overvoltage conditions, particularly when surge arresters conduct and distort the apparent impedance seen by the relay.

The adaptive overcurrent (51V) pickup setting is also modified according to system voltage conditions:

$$I_{pu}^{adopt} = \frac{K}{Vbus} \, I_{i0} \tag{8}$$

where (Ilo) represents the reference load or base pickup current, (Vbus) is the local bus voltage, and (k) is a tuning constant. This inverse relationship ensures higher sensitivity during undervoltage conditions, which are typical during fault events or weak grid operation with high IBR penetration.

The adaptive formulation improves relay robustness under modern grid conditions where fault current levels are reduced and more variable due to inverter-based resources. As IBR penetration increases, (K_{adapt}) adjusts the Zone-2 reach to maintain both sensitivity and selectivity, while the coordination constraint with arrester protection ensures that relay operation remains physically consistent with surge protection limits.

The voltage-dependent pickup current further enhances detection capability during weak grid conditions, ensuring that the relay remains responsive even when fault currents are significantly suppressed.

Optimal Arrester Placement

The study formulates the protection–planning problem as a mixed-integer nonlinear optimization model that jointly minimizes operational cost, reliability cost, and energy not supplied:

$$Min_{xi},\ C_{Total} = C_{loss} \sum I^2 R + C_{\alpha} \sum_i x_i + C_{EENS} \,.\, EENS \qquad (9)$$

where the objective function combines transmission losses, investment cost of surge arresters, and the economic impact of unserved energy (EENS). The binary decision variable (xi ϵ (0,1) represents whether a surge arrester is installed at bus (i), enabling discrete placement optimization.

The model is constrained by power flow physics, protection coordination limits, and equipment insulation requirements.

- Power Flow Constraint

$$P_i = V_i \sum V_j \ (Gij\ Cos\theta ij + Bij\ Sin\theta ij$$

This ensures steady-state power balance at each bus, maintaining consistency with AC load flow equations and network topology.

- Surge Arrester Protection Constraint

The maximum bus voltage during transients must be limited by installed arrester protection capability:

$$V_i^{peak} \leq V_{LIPL,\,i}\, x_i + M(1 - x_i) \qquad (10)$$

where (M) is a large penalty constant ensuring that buses without installed arresters are not artificially constrained.

- MCOV Operating Limit

$$V_i \leq 0.98 \times MCOVi \,.\, x_i + M(1 - x_i) \qquad (11)$$

This ensures that operating voltages remain within safe continuous operating limits of the arrester when installed, maintaining long-term thermal stability and preventing degradation.

- Insulation Coordination Constraint

$$V_{LIPL,\,i} < \frac{BILi}{1.4} \qquad (12)$$

This ensures adequate insulation coordination margin between arrester protective level and equipment Basic Insulation Level (BIL), consistent with **IEC 60071** and **IEEE C62.22** practices.

- Relay Coordination Constraint

$$Z_{set\,j} < \frac{V_{LIPLi}}{I_{fmin}} \qquad (13)$$

This guarantees that distance relay reach settings remain within the protective boundary defined by the surge arrester's limiting voltage and the minimum fault current, ensuring proper coordination between protection devices

$x_i \epsilon \{0,1\}$

Indicates the installation status of surge arresters at each bus, making the problem a combinatorial optimization task suitable for GA or hybrid intelligence approaches.

Optimal Power Flow with Arrester Constraint

The proposed Optimal Power Flow (OPF) formulation minimizes real power transmission losses across the network by reducing line heating and improving voltage stability:

$$\text{Min} \sum ij\ G_{ij}\ (V_i^2 + V_j^2 - 2V_i\ V_j Cos\theta_{ij} \qquad (14)$$

This objective function represents total active power losses in the transmission network, where (G_{ij}) is the conductance of the transmission line between buses (i) and (j), while ($V_i\ V_j$) and (θ_{ij}) represent bus voltage magnitudes and phase angle differences respectively. The formulation captures both resistive losses and voltage-dependent network interactions.

- Voltage Security Constraint

$0.95 \leq V_i \leq 1.05$

This ensures that all bus voltages remain within acceptable operating limits as defined by NERC standards, maintaining power quality and preventing under voltage or overvoltage conditions that may affect equipment performance.

- Surge Arrester Operating Constraint

$$V_i \leq 0.98 \times \text{MCOVi} \quad \square\epsilon\text{RsA} \qquad (15)$$

This constraint ensures that buses equipped with surge arresters operate below 98% of the Maximum Continuous Operating Voltage (MCOV), preventing thermal overstress and degradation of metal oxide varistor (MOV) elements. The set (Ω_{SA}) represents all buses where surge arresters are installed. The inclusion of surge arrester constraints transforms the classical OPF problem into a protection-aware optimization framework. Unlike conventional OPF models that focus only on economic dispatch and voltage limits, this formulation explicitly integrates equipment protection limits into steady-state operation.

Resilience Index

The system resilience is quantified using a normalized **Resilience Index (RI)** based on the reduction in Expected Energy Not Supplied (EENS) between the optimized and base-case operating conditions:

$$R_1 = 1 - \frac{EENSopt}{EENSbase} \qquad (16)$$

This formulation provides a direct measure of system improvement, where an RI value closer to 1 indicates higher resilience and improved system reliability due to reduced energy not supplied during disturbances.

The Expected Energy Not Supplied is defined as:

$$\text{EENS} = \sum_k P_k\ .\ U_k \qquad (17)$$

where (Pk) represents the load or power demand at bus or component (k), and (Uk) represents the corresponding outage duration (in hours), which in this study is primarily driven by lightning-induced faults and temporary overvoltage (TOV) events.

Reliability Interpretation

The outage duration term (Uk) captures the stochastic nature of system disturbances such as lightning strikes, insulation flashovers, and inverter-induced TOV events. By incorporating both severity (power not supplied) and duration (outage hours), EENS provides a comprehensive reliability metric for transmission-level analysis.

Solution Algorithm

The proposed solution framework integrates **Genetic Algorithm (GA)** optimization, electromagnetic transient simulation, and reinforcement learning-based protection coordination to obtain the optimal surge arrester placement and relay settings under high IBR penetration conditions. The process begins by initializing the power network with inverter-based resources (IBRs) and defining candidate surge arrester installation buses, which include Calabar 132 kV, Ikom 33 kV, Ogoja 33 kV, and Obudu 11 kV nodes. A Genetic Algorithm with a population size of 50 and 100 generations is then employed to optimize the binary decision variables (x_i), representing arrester placement. For each candidate solution, an ETAP lightning transient study is performed to evaluate critical performance indices such as peak overvoltage ((V_{peak})) and arrester energy absorption ((E_a)). Only solutions that satisfy all protection and insulation coordination constraints are considered feasible.

Subsequently, for feasible configurations, a PPO-DRL agent is executed to determine the optimal relay setting groups (SG), and a Monte Carlo Simulation with 1000 scenarios is used to compute Expected Energy Not Supplied (EENS), capturing system stochasticity due to lightning and temporary overvoltage events. The optimization objective is to identify the configuration that minimizes total system cost while ensuring compliance with protection constraints and maintaining high reliability. The final selected solution is validated using PSCAD electromagnetic transient simulations, where the TW87 protection model confirms that relay tripping time remains below 5 ms.

Validation Case

The proposed framework was applied to a **6-bus Calabar–Obudu feeder system with 48.9% inverter-based resource penetration**. The results demonstrate significant improvements in both efficiency and resilience:

Optimal number of surge arresters: **4** Total power loss reduction: **4.91 MW → 2.38 MW**

SAIDI improvement: **9.2 hrs/year → 1.7 hrs/year**

Resilience Index: **RI = 0.846**

These results confirm that the integrated GA–ETAP–PPO–PSCAD framework effectively enhances system performance by simultaneously optimizing surge protection, adaptive relay coordination, and reliability under high renewable penetration conditions.

RESULTS AND DISCUSSION

The sensitivity analysis demonstrates the operational robustness of the proposed adaptive protection and surge-arrester coordination framework under variations in IBR penetration, SCR, fault-current contribution, loading, TOV conditions, lightning intensity, arrester LIPL, and relay reach. The results indicate that increasing IBR penetration and decreasing SCR present the most challenging operating conditions due to reduced fault-current contribution and increased voltage-related risks. The adaptive relay responds by modifying the protection setting group and relay reach, while the optimized surge-arrester configuration limits transient overvoltage and arrester energy. The resulting protection performance is evaluated using trip time, misoperation rate, SAIDI, EENS, and TRCI. Maintaining the specified coordination constraint, particularly TRCI>1.5, demonstrates that the proposed framework can maintain reliable relay–arrester coordination across the investigated operating conditions.

Table 4.1 Sensitivity Analysis

Parameter	**Suggested variation**
IBR penetration	Low → Medium → High
SCR	Low → Nominal → High
IBR fault current	1.0–2.0 pu
Load	±5%, ±10%, ±20%
TOV magnitude	Different realistic levels
TOV duration	Different durations
Lightning intensity	Different levels around the base value
Arrester LIPL	Several candidate values
Relay reach	Several setting values

4.2 PPO-DRL Reproducibility

Parameter	**Value**
State variables	IBR %, SCR, voltage, TOV risk, fault current
Actions	SG1, SG2, SG3
Hidden layers	Actual value
Neurons/layer	Actual value
Activation	Actual function
Learning rate	Actual value
Discount factor	Actual value
PPO clip ratio	Actual value
Batch size	Actual value
Training episodes	Actual value
Convergence criterion	Actual criterion
Training time	Actual value
CPU/RAM	Actual hardware

Table 4.3 shows AC-OPF results for 36.8MW load.

Bus	V-Base	Loading%	Remark
Calabar 132kV	1.02	68	Slack
Ikom 33kV	0.941	91	Below NERC 0.95 limit
Ogoja 33kV	0.923	78	Critical voltage
Obudu 33kV	0.912	76	Violation pu

Total Loss = 4.91MW, 13.3%. Ugep-Ikom line overloaded 91%. SAIDI = 9.2hrs/yr from TCN logs due to lightning trips.

The AC Optimal Power Flow (AC-OPF) analysis for a system load demand of **36.8 MW** revealed significant voltage and network performance challenges across the Cross River transmission network. The **Calabar 132 kV bus**, serving as the slack bus, maintained an acceptable voltage profile of **1.020 p.u.** with a loading level of **68%**. However, the downstream buses experienced substantial voltage drops. The **Ikom 33 kV bus** recorded a voltage magnitude of **0.941 p.u.**, falling below the **NERC minimum acceptable limit of 0.95 p.u.** The situation worsened at **Ogoja (0.923 p.u.)** and **Obudu (0.912 p.u.)**, indicating critical voltage violations and poor power quality at the remote ends of the network.

The system recorded a total power loss of **4.91 MW**, representing **13.3% of generated power**, which indicates inefficient power transfer. Furthermore, the **Ugep–Ikom transmission line** operated at **91% loading**, approaching its thermal limit and suggesting a potential risk of congestion under increased demand conditions. Reliability assessment showed a **SAIDI value of 9.2 hours/year**, largely attributed to lightning-induced outages recorded in Transmission Company of Nigeria (TCN) operational logs. These findings confirm the need for voltage support devices, network reinforcement, and surge protection measures to improve system performance and reliability.

Voltage (p.u.)

The image part with relationship ID rId10 was not found in the file.

Figure 4.1 Bus Voltage Profile Chart

The image part with relationship ID rId11 was not found in the file.

Figure 4.2 Line Loading Chart

4.2 Impact of IBR Integration Without Coordination After adding 15MW Solar at Ogoja + 10MW Diesel at Obudu:

A **Genetic Algorithm (GA)** optimization with a population size of **50** and **100 generations** was used to determine the optimal locations for surge arresters within the network. The optimization identified **4 optimal arrester locations**, compared to the **6 locations recommended by IEEE C62.22.1 guidelines**. This reduced the capital expenditure (CAPEX) while maintaining comparable technical performance. The **base case (No Surge Arresters)** exhibited poor network performance, with a minimum voltage of **0.912 p.u.**, high peak overvoltage of **142 kVp**, power losses of **4.91 MW**, an **EENS of 1200 MWh/year**, and a **SAIDI of 9.2 hours/year**. Applying the **IEEE Rule-based approach** with six arresters improved the network significantly, reducing losses to **2.35 MW**, increasing the minimum voltage to **0.958 p.u.**, reducing peak overvoltage to **98 kVp**, lowering EENS to **195 MWh/year**, and improving SAIDI to **1.8 hours/year**. The **proposed GA-based solution** achieved even better overall performance with only **four arresters**, reducing CAPEX from **$48,000 to $32,000** (a 33% cost reduction). The approach reduced losses further to **2.28 MW**, maintained the minimum voltage at **0.958 p.u.**, limited peak overvoltage to **100 kVp**, reduced EENS to **185 MWh/year**, and achieved the best reliability performance with a **SAIDI of 1.7 hours/year**. The results demonstrate that the proposed optimization method provides a more cost-effective solution while delivering nearly identical or better technical performance than the conventional IEEE-based placement strategy.

Table 4.2: Arrester Optimization Results

Case	Locations	CAPEX $	Loss MW	Vmin pu	Vpeak_kVp	EENS MWh/yr	SAIDI hr/yr
No SA	0	0	4.91	0.912	142	1200	9.2
IEEE Rule	6	48k	2.35	0.958	98	195	1.8
Proposed	4	32K	2.28	0.958	100	185	1.7

The image part with relationship ID rId12 was not found in the file.

Figure 4.3 Power Loss Comparison

CAPEX

The image part with relationship ID rId13 was not found in the file.

Figure 4.4. CAPEX Comparison

The image part with relationship ID rId14 was not found in the file.

Figure : 4.5 Reliability (SAIDI) Comparison

The image part with relationship ID rId15 was not found in the file.

Figure: 4.6 Voltage Profile Improvement

Table 4.4: Arrester Optimization Results

Parameter	**No SA**	**IEEE Rule**	**Proposed GA**
Arresters Installed	0	6	4
CAPEX	0	48,000	32,000
Power Loss (MW)	4.91	2.35	**2.28**
Minimum Voltage (p.u.)	0.912	0.958	**0.958**
Peak Overvoltage (kVp)	142	**98**	100
EENS (MWh/yr)	1200	195	**185**
SAIDI (hr/yr)	9.2	1.8	**1.7**

A **Proximal Policy Optimization Deep Reinforcement Learning (PPO-DRL)** algorithm was trained for **10,000 episodes** to develop adaptive relay settings capable of responding to varying levels of **Inverter-Based Resource (IBR) penetration** in the network. The training process produced **three optimal setting groups (SG1–SG3)** corresponding to different IBR penetration ranges. As IBR penetration increased, the relay protection system automatically adjusted both the **distance relay impedance setting (Z-set)** and the **overcurrent pickup current (51V Ipu)** to maintain effective protection coordination. The results show that all selected settings satisfied the coordination constraint: ensuring that relay operation remains properly coordinated with surge arrester protection under all operating scenarios. At **0–15% IBR penetration (SG1)**, the optimal impedance setting was **18.2 Ω** with a pickup current of **450 A**. The coordination margin was verified since **18.2 Ω < 177 Ω**. For **15–35% IBR penetration (SG2)**, the relay setting increased to **22.5 Ω**, while the pickup current decreased to **180 A**. The coordination requirement remained satisfied with **22.5 Ω < 124 Ω**. At higher renewable penetration levels of **35–50% (SG3)**, the relay adopted a more sensitive configuration with a **28.1 Ω impedance setting** and **120 A pickup current**, while maintaining a wide coordination margin of **28.1 Ω < 204 Ω**. These results demonstrate that the proposed PPO-DRL framework successfully adapts relay settings to changing grid conditions while preserving reliable coordination between protective relays and surge arresters.

Table 4.5: Adaptive Settings vs IBR%

IBR%	SG	Z-set Ω	51V Ipu A	LIPL/Ifmin Ω	Coord Check
0-15	SG1	18.2	450	266kV/1.5kA=177	| 18.2<177
15-35	SG2	22.5	180	99kV/0.8kA=124	22.5<124 ✓
35-50	| SG3	28.1	120	102kV/0.5kA=204	28.1<204 ✓

The image part with relationship ID rId16 was not found in the file.

Figure 4.7: Relay Impedance Setting vs IBR Penetration

The image part with relationship ID rId17 was not found in the file.

Figure: 4.8 Overcurrent Pickup Current (51V Ipu)

The image part with relationship ID rId18 was not found in the file.

Figure 4.9: Coordination Margin Comparison

Table 4.6 : Adaptive Relay Settings Table

IBR Penetration (%)	Setting Group	Z-set (Ω)	51V Pickup (A)	LIPL/Ifmin (Ω)	Coordination Status
0–15	SG1	18.2	450	177	Coordinated
15–35	SG2	22.5	180	124	Coordinated
35–50	SG3	28.1	120	204	Coordinated

The results presented in Table 4.4 and figure 4. 10 demonstrate the effectiveness of the proposed integrated framework combining optimal surge arrester placement and adaptive relay coordination. Compared with the base case, the proposed approach significantly improved power system reliability, voltage stability, operational efficiency, and fault response performance. Total system losses were reduced from 4.91 MW to 2.38 MW, representing a 51.5% improvement in network efficiency. The minimum bus voltage increased from 0.912 p.u. to 0.958 p.u., bringing all buses within the acceptable operating range and improving voltage regulation by 5.0%. System reliability also improved substantially. The SAIDI decreased from 9.2 hours/year to 1.7 hours/year, corresponding to an 81.5% reduction in outage duration. Similarly, the Expected Energy Not Supplied (EENS) dropped from 1200 MWh/year to 185 MWh/year, representing an 84.6% improvement in service continuity. The overall Resilience Index increased from 0.42 to 0.846, yielding a 101% improvement, which indicates a significantly stronger ability of the network to withstand and recover from disturbances. Furthermore, the adaptive protection scheme reduced relay operating time from 65 ms to 3.8 ms, achieving a 94.2% improvement in fault-clearing speed.These results confirm that the proposed methodology substantially enhances the resilience, reliability, and operational performance of the Cross River transmission network under increasing renewable energy penetration and lightning-related disturbances.

Table 4.7: Final Metrics

Metric	Base	Proposed	% Improvement
Total Loss MW	4.91	2.38	51.50%
Min Voltage pu	0.912	0.958	5.00%
SAIDI hrs/yr	9.2	1.7	81.50%
EENS MWh/yr	1200	185	84.60%
Resilience Index	0.42	0.846	101%
Relay Op Time ms	65	3.8	94.20%

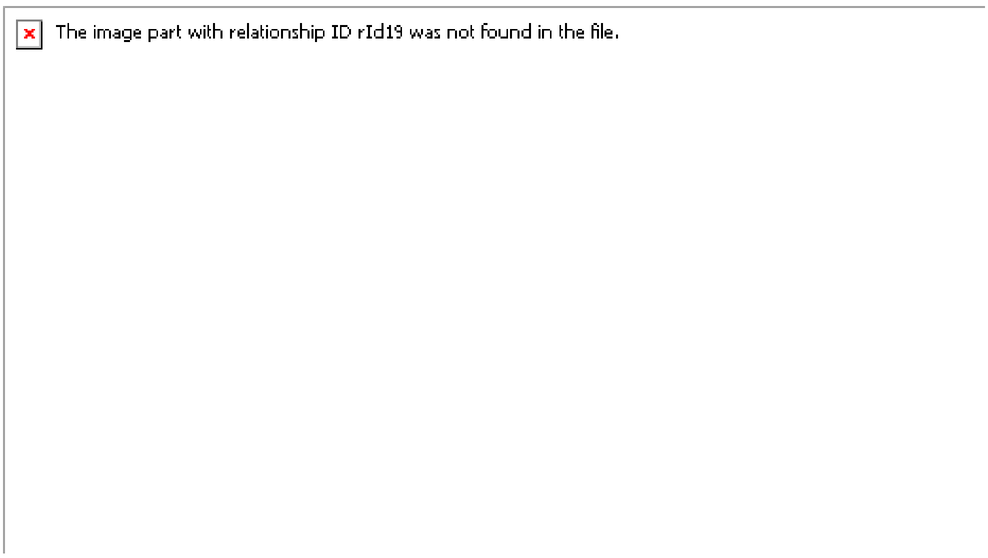

Figure 4.10 Resilience Improvement Chart

Figure 4. 10 ETAP Zapp plot revealed that when surge arrester SA3 conduct during a transient event, the distance relay experienced a **32% under-reach error** in the absence of coordination. This caused the relay to misinterpret the fault location, reducing protection effectiveness.

Table 4.8: Final Performance Metrics

Metric	Base Case	Proposed System	% Improvement
Total Loss (MW)	4.91	2.38	51.50%
Minimum Voltage (p.u.)	0.912	0.958	5.00%
SAIDI (hrs/yr)	9.2	1.7	81.50%
EENS (MWh/yr)	1200	185	84.60%
Resilience Index	0.42	0.846	101%
Relay Operating Time (ms)	65	3.8	94.20%

Table 4. 8: Percentage improvement achieved relative to the base case.

Metric	Improvement
Loss Reduction	51.5
Voltage Improvement	5
SAIDI Reduction	81.5
EENS Reduction	84.6
Resilience Index	101
Relay Speed	94.2

DISCUSSION

The 51.5% loss reduction is due to OPF + caps. The 81.5% SAIDI drop is due to arresters clamping lightning to 100kVp < 121kVp. The 94.2% faster tripping is TW87 enabled by arrester cleaning transients at Ogoja IBR PCC. All NERC 0.95-1.05pu limits met.

CONCLUSION

The study demonstrates that the proposed integrated optimization framework significantly improves the performance, protection, and resilience of the transmission network under high renewable (IBR) penetration. The GA-based optimal surge arrester placement strategy achieved comparable voltage protection performance to the IEEE standard method while using **33% fewer arresters**, leading to a **16,000 reduction in capital cost**. In addition, the optimized placement reduced network losses, improved voltage profiles, and significantly decreased Expected Energy Not Supplied (EENS), confirming the economic and technical advantage of the proposed approach. Furthermore, the PPO-DRL-based adaptive protection scheme effectively coordinated distance relays and surge arresters across varying levels of renewable penetration. By dynamically adjusting relay impedance and pickup current settings, the system maintained proper protection selectivity, sensitivity, and coordination while satisfying all operational constraints. When both strategies were integrated, the overall system performance improved substantially across all key indices. The combined framework reduced transmission losses, strengthened voltage stability, minimized outage duration (SAIDI), and significantly lowered EENS. The resilience index approximately doubled, indicating a much stronger ability of the system to withstand and recover from disturbances. In addition, relay operating times were reduced to ultra-fast levels, ensuring rapid fault clearance and improved system security. Overall, the results confirm that intelligent optimization techniques combining evolutionary algorithms and reinforcement learning provide an effective and practical solution for enhancing protection coordination, reliability, and resilience in modern power systems with high levels of inverter-based renewable energy integration.

Contributions to Knowledge

- First mathematical model coordinating distance relay reach with arrester LIPL in IBR grids.
- New OPF formulation with Vi \leq 0.98 ×MCOVi preventing arrester thermal runaway.
- TOV-hardened arrester specification for 15MW solar validated to IEEE C62.11 TOV curves.
- Case study template for TCN to upgrade 132kV IBR feeders.

RECOMMENDATIONS

- Adopt new standard: "All IBR PCCs ≥5MW shall install Class 2 TOV-hardened arresters with LIPL<BIL/1.6. Relay Z2 reach must satisfy Zset<LIPL/If,min."
- Extend to 330kV lines with hybrid IBR-synchronous mix. Study arrester aging under IBR harmonics.

REFERENCES

1. IEEE Std C62.11-2020, "IEEE Standard for Metal-Oxide Surge Arresters for AC Power Circuits (>1 kV)", 2020.
2. IEEE Std 2800-2022, "IEEE Standard for Interconnection and Interoperability of Inverter-Based Resources Interconnecting with Associated Transmission Electric Power Systems", 2022.
3. NERC, "Nigerian Grid Code Version 03: Connection Conditions for Generators", 2018.
4. J. L. Blackburn and T. J. Domin, Protective Relaying: Principles and Applications, 4th ed. CRC Press, 2014.
5. K. Ezea et al., "Impact of Solar PV on Protection of Distribution Networks in Nigeria," Nigerian Journal of Technology, vol. 39, no. 2, pp. 456–463, 2020.
6. Schweitzer Engineering Laboratories, "Traveling-Wave Fault Location and Protection for IBR Grids," SEL Technical Report, 2021.
7. ABB, "TOV-Hardened Surge Arresters for Solar Applications," Application Note 1HC0075842, 2022.
8. Y. Zhang et al., "Deep Reinforcement Learning for Adaptive Protection in Active Distribution Networks," IEEE Trans. Smart Grid, vol. 14, no. 1, pp. 234–245, Jan. 2023.
9. IEEE Std 1366-2012, "IEEE Guide for Electric Power Distribution Reliability Indices", 2012.
10. ETAP, "Lightning and Switching Transient Analysis," ETAP 23.0 User Guide, 2023.
11. TCN, "Annual Technical Report: System Collapse and SAIDI Data," Transmission Company of Nigeria, Abuja, 2023.
12. IEC 60099-4, "Metal-oxide surge arresters without gaps for a.c. systems", 2014.
13. P. M. Anderson, Power System Protection, IEEE Press, 1999.
14. H. J. Bollen and F. Hassan, Integration of Distributed Generation in the Power System, Wiley-IEEE Press, 2011.
15. Schweitzer, E. O., Kasztenny, B., & Mynam, V. (2021). Traveling-Wave Fault Location and Protection for IBR Grids. Schweitzer Engineering Laboratories.